Characterization of Cloud Cover with a Smartphone Camera

A.V. Parisi[1,*], N. Downs[1], D. Igoe[1] & J. Turner[1]

[1]Faculty of Health, Engineering and Sciences, University of Southern Queensland, Toowoomba. Australia

[*]Corresponding author: parisi@usq.edu.au

Keywords: solar radiation; clouds; smartphone; sky camera

Abstract

A smartphone sky camera and associated image analysis algorithm has been developed and validated for the determination of the percentage of cloud cover. This provides the total cloud cover and the percentage of thick and thin cloud in the image. The system has been validated and tested using supervised image classification for a range of cloud types and cloud cover ranging from 4% to 98% and solar zenith angles between 6^{o} and 49^{o}. Additionally, this system provides the percentage of total cloud and thick and thin cloud in proximity to the solar disc. The size of the errors is comparable to those associated with the cloud fractions determined with commercial sky camera systems. The benefits of increasing the availability of cloud fraction measurements through the system described include the potential to develop improved local ultraviolet index and weather forecasts and contribute toward better understanding of local trends in cloud patterns that is required to be considered in the generation of solar energy.

Introduction

Cloud cover and type for a given site, date and time are the major influences on ground based solar irradiances. Component water droplets and ice crystals may absorb or scatter incident direct and diffuse solar radiation influencing the ratio of both components measured at the earth's surface[1]. Cloud cover affects the measured solar radiation depending on the cloud type, the total optical path at the time of measurement, total sky distribution, and cloud proximity relative to the solar disc[1]. In addition to the influence on the solar irradiance, there is also an associated wavelength dependence[2,3,4]. In the majority of cases, clouds reduce the solar radiation reaching the earth's surface. However, there are cases with certain types and configuration of cloud when the irradiances of the shorter waveband ultraviolet are enhanced above that of a cloudless day[5,6]. Traditionally, the fraction of cloud cover has been provided by trained observers, with the amount of cloud provided in octas (or sky cover measured in eighths)[7]. A review of cloud detection methods has been previously undertaken[8]. One group of these cloud detection methods is based on taking digital images of the sky and using image processing algorithms to determine the level of cover. Sky cameras that image a wide field of view, coupled with image analysis have provided a means for the determination of the amount of cloud cover with a high temporal resolution[9,10,11,12]. Additionally, the relevant calibration has allowed the extraction of radiance information from all-sky images[13,14].

Several automated sky cameras have been developed for the evaluation of cloud characteristics. An automated Whole Sky Imaging system for the determination of both the daytime and night time cloud cover has been reported[9,10]. A sky camera system with 16 bit resolution and image capture up to every 1.6 seconds for use in short-term forecasting of solar power generation has been reported[15]. A Sun Centred Sky Camera has been reported[16,17] as providing approximately 82% correct identification of the cloud fraction and

77% correct identification of solar obstruction. This camera was installed on a tracker keeping the sun in the centre of the image throughout the day. Another form of upward looking sky camera is the upward looking fish eye lens camera or Whole Sky Camera instrument[18]. This instrument has a shadow band that runs east-west which can be periodically adjusted for the seasonal change in solar altitude. A red/blue pixel ratio was used to count the proportional area of cloud cover, classifying image pixels as either 'cloud' or 'no cloud'. Pixel ratios above a threshold value of 0.6 were used to designate image pixels as cloudy or below this as cloud-free pixels. A digital camera with a 36^{o} field of view[19] was employed at a high latitude site with cloud classification based on the saturation component of the intensity, hue and saturation space, with the results compared to the classification of the amount of cloud cover by two meteorologists.

An automated sky imager with a 160^{o} field of view has been developed and is commercially available in the form of the Total Sky Imager (model TSI440 and model TSI880, Yankee Environmental Systems, MA, USA)[18,20]. These instruments are based on a digital camera pointing downwards onto a mirrored hemispherical dome. The dome has a black strip to block the solar disc to prevent saturation of the charge-coupled device (CCD) camera as the dome rotates during the day. In the image, each pixel is analysed for the red/blue ratio and a threshold applied to this to establish if they are a cloud or no cloud pixel. An extension to the application of the Total Sky Imager has been research on the use of a pair of separated Total Sky Imager instruments for the determination of the cloud base height[21,22].

Cloud modification factors have been employed in research to establish relationships between amounts of cloud and irradiances in different wavebands[23]. The cloud modification factor is defined as the ratio between the measured irradiance in a specific waveband and the

corresponding clear sky irradiance for the same solar zenith angle and atmospheric conditions.

Satellite cloud data are available, for example from the Moderate Resolution Imaging Spectroradiometer on a satellite with a sun synchronous orbit. The Moderate Resolution Imaging Spectroradiometer provides information on cloud parameters and cloud fraction[24]. The temporal resolution of this data is daily, but it provides almost global geographical coverage. However, the spatial resolution is of the order of 250 to 500 m in the visible waveband and local cloud data for a specific site requires the use of ground based instrumentation. The satellites on geostationary orbits such as the Geostationary Operational Environmental Satellite and the Meteosat series provide data with a higher temporal resolution, but with a lower spatial resolution[8]. An example of the application of this data includes the study of three years of Total Sky Imager data from a Southern Hemisphere site at 20^{o} S that were analysed to determine local cloud cover[25]. A comparison of this with satellite derived cloud data showed that the satellite data typically underestimated the cloud cover, but it was possible to establish a relationship that related one to the other.

For both the Whole Sky Camera and the Total Sky Imager, the ratio of the red/blue pixels is employed to distinguish between no cloud and cloud covered sky as the red pixel values are relatively small for parts of the sky that are cloud free due to the minimal Rayleigh scattering of these wavelengths in a cloud free atmosphere. A problem with this method includes the incorrect classification of cloud pixels in proximity to the solar disc for the cases of a bright sky. This is due to scattering by aerosols and is worse for cases where there are high atmospheric aerosols or at lower solar elevations which increase the optical path[18,26]. Various thresholds have been employed such as 0.6 for the Whole Sky Camera system[18].

Alternatively, a variable threshold has been employed in the Total Sky Imager system[18]. Another approach employs the calculation of a difference of the blue and red pixels and a difference threshold instead of using a ratio[27]. The research of Heinle et al.[27] reports that employing a threshold on the difference between the two channels outperforms an approach that uses a threshold on the ratio of the two channels.

The previous research has shown that the use of sky cameras and image processing can provide the fractional cloud cover with the errors being no worse than that for human observations[18]. The advantages of a sky camera over human observations are the increased frequency of non-subjective observations and the improved spatial resolution compared to satellite observations. However, the cost of the current sky cameras can at times be a hurdle for the widespread use of these devices. Earlier research has investigated the use of smartphone sensors in ultraviolet A radiation measurement[28-32]. This paper extends this earlier research and describes a sky camera based on a smartphone to collect a sky image of wide angle, along with the analysis of the sky images to determine the cloud fraction and the fraction of cloud in proximity to the solar disc.

Methods

Image Collection

Images of the sky were collected with the camera on a smartphone (Apple iPhone 5) fitted with a fish eye lens[33] over the phone's second camera. Although, an iPhone was employed in this research, any make and model smartphone that produces a jpg file could have been employed. The second camera was employed as it provides access to the shutter button on the phone's screen. The fish eye lens is readily available to purchase online, is inexpensive and can be readily attached over the smartphone camera lens by firstly fixing an adhesive metal

ring around the camera sensor to which the lens attaches magnetically. A light tight coupling of the lens to the phone was ensured by placing a thin rim of pliable ‘blu tack’ at the junction between the lens and the camera. The smartphone sky camera setup is shown in Figure 1 with the fish eye lens attached to the phone and the black occultation disc manually positioned to obscure the direct solar radiation from the sensor. The wire suspending the occultation disc was inserted into a small block of wood for stability, however anything that held the wire could be employed.

The modified smartphone was used to collect sky images on a horizontal plane on a relatively unobstructed building roof at the University of Southern Queensland Toowoomba Campus (27.6^{o} S, 690 m a.s.l), Australia. A series of forty images were collected over a solar zenith angle range of 6^{o} to 49^{o} degrees and for cloud cover ranging from 4% to 98%.

The fish eye lens attachment provides an approximate 160^{o} field of view, however the image is truncated at the top and bottom sides, corresponding to the east and west sides. These truncated parts of the image result in approximately a 100^{o} field of view in the east-west direction. For each image collected, the solar disc was manually obscured with a black occultation disc of 28 mm diameter that was suspended 60 mm above the top of the lens on a goose neck shaped thin wire. The number of pixels obstructed varies with the solar zenith angle and in the images in this research is of the order of 3.5%. The number of pixels obscured by the wire suspending the occultation disc were minimal. The occultation disc was positioned manually over the lens to shadow the sensor from the direct sun and the shutter on the screen then pressed for image collection. A small red circle of approximately 4 mm diameter was adhered to the centre of the underside of the black occultation disc in order to allow identification of the centre of the solar disc in the image analysis described in the next

section. The positioning of the occultation disc is not possible for totally overcast skies when it is not possible to see the shadow of the disc. However, it is possible in all other cases when there is at least a partial shadow cast.

Image Analysis

The images collected are stored in jpeg format and for the phone employed are recorded in 960 rows and 1,280 columns (~ 1.2 MegaPixels). The jpeg images were stored and processed in *Matlab*[34] as an indexed image where each pixel is assigned an integer (or image map marker) that points to the relevant red, green and blue (RGB) values of an 8-bit (256 row) colour map or matrix of three columns of floating point numbers between 0 and 1 to specify the red, green and blue components of each colour to be referenced by corresponding image pixels.

For each image, the approach employed was to analyse the red, green and blue values for each sky image pixel to provide a classification of clouded sky regions, where for blue sky there is a significantly higher proportion of blue than red due to preferential atmospheric scattering of short wavelength radiation compared with cloud cover which tends to scatter light independently of wavelength. Pixels covered by the black occultation disk and those lying outside the circular fish eye lens were digitally masked (red=0, green=0, blue=0) before each image was processed. The fraction of cloud cover was calculated employing the approach of Long et al.[18]:

$$f = \frac{N_{cloud}}{N_{total}} \quad (1)$$

where N_{cloud} is the number of pixels that were classified as being cloud and N_{total} is the number of pixels in the sky image, not counting masked pixels. The approach employed by the Total Sky Imager[18] was utilised here where no correction was made for the slightly

different solid angle view of each pixel compared to the neighbouring pixel. Long et al.[18] evaluated the error in the fractional cloud cover of not applying this correction as only marginally greater than 1%.

Each image was analysed using a specifically written algorithm for *Matlab*[34] employing Matlab's Image Processing Toolbox. Smartphone images were transferred to a computer with the image analysis software. The approach employed in the image analysis was to analyse the difference between the blue and red values for each pixel as done by Heinle et al.[27], rather than the ratio of the two values. The difference between the blue and red values will be referred to in the following as blue-red. The image analysis process is described in the steps below.

- The maximum difference between the blue and red values was determined and the contrast of the colour map increased with this value employed to scale the blue-red to a maximum value of 1.
- The parts of the colour map that refer to the red dot on the black occultation disc were established to determine the position of the solar disc. Due to the differences in the brightness of different images, this was determined by considering the ratio of the red to the blue values and identified as the red disc if the ratio was greater than 2 and the red pixel map value was above 0.2.
- The parts of the colour map for pixels that correspond to no image due to being outside of the field of view or being hidden by the occultation disc were determined. These were determined by considering the difference between the red and green values and if less than 0.04 and the blue pixel map value was low at less than a threshold, this was identified as no image. The threshold employed was 0.3 for the

majority of cases, except for images with darker storm clouds when it was lowered to 0.23.

- The remaining parts of the colour map belonging to the image with cloud were determined as cloud based on a threshold applied to the blue-red values. This threshold to determine between cloud and sky was employed as 0.9 for bright skies and 0.65 otherwise. The threshold value for bright skies was the maximum blue-red value being greater than 0.4. The pixels classified as cloud were further classified as thin cloud or thick cloud based on a threshold of 0.45 applied to the blue-red values. This threshold was determined by the analysis of images for a solar zenith angle over 6 to 49 degrees and low to high amounts of cloud cover. These thresholds may require minor adjustments with a different smartphone camera or other atmospheric conditions.
- The colour map values were allocated as blue, black, red, white or green corresponding to sky, no image, solar disc, thick cloud and thin cloud respectively.
- The image was now analysed to count the number of pixels classified as sky, no image, thick cloud and thin cloud, allowing the percentage of sky, thin cloud, thick cloud and total cloud to be calculated. The parts of the image classified as no image or red as corresponding to the solar disc were not included in the calculation.
- A circle with a radius of 250 pixels was determined around the position of the solar disc and within this circle the number of pixels classified as sky, thick cloud and thin cloud were determined and counted to calculate the percentage of sky, total cloud, thick cloud and thin cloud. Again, the parts of the image classified as no image or red were not included in the calculation.

Validation

The validation of the sky image classification was undertaken with the *MultiSpec* image analysis software[35]. Each of the jpeg images to be validated was opened in *MultiSpec* and supervised classification of each image undertaken. Supervised classification requires the user selection and identification of representative parts of an image that are known as training sets, followed by software classification of pixels in the image according to the respective training set features that the pixel most closely resembles. Training sets were established for thick cloud, thin cloud, sky, the red dot specifying the solar position and the other image components not belonging to the sky image. The maximum likelihood classifier was employed for classification of each pixel. For the cases where visual inspection of the classified image showed that there were parts of the image which were not correctly classified, a second iteration with the definition of further training sets was employed to improve the classification. The number of pixels classified in each category was provided by *MultiSpec* and these numbers were employed to calculate the percentages of total cloud, thick cloud, thin cloud and sky in each image. These classifications were compared to those resulting from the *Matlab* algorithm.

For the circle of 250 pixels around the sun, a separate image was generated from the original value using *MatLab* with the pixels more than 250 pixels from the solar disc masked as black for two test images, one with a solar zenith angle of 6^{o} and one with a solar zenith angle of 11^{o}. Training sets were established using *Multispec* for the classification of the pixels within these images for comparison to those resulting from the *Matlab* algorithm.

Results and Discussion

A sample of an image using this process is shown in Figure 2. The occultation disc masks a number of pixels centred around the sun in the image in a similar manner to the bands on the Whole Sky Camera and Total Sky Imager systems[18]. The top and bottom of the image, corresponding to the east west axis were truncated due to the image produced by the fish eye lens being larger than the sensitive area of the smartphone camera sensor. However, the truncated image regions are for the parts of the sky closer to the horizon and provides a field of view of approximately 100 degrees for the east west axis.

The smartphone sky camera images for low and mid amounts of cloud are shown in Figure 2 and Figure 3, with the image on the right in each figure showing the processed image. The processed images show the thick cloud as white, the thin cloud as green and the sky as blue. The parts of the image that are masked due to the occultation disc or that are outside of the fish eye image area are shown in black, with the centre of the sun depicted by the red dot. There are pixels of the images where there is cloud that are saturated for the red value and the blue value. However, the process employed in this paper where the blue-red value is calculated allows the classification of these pixels as thick cloud.

The percentages of total cloud, thick cloud and thin cloud in the whole image and within a 250 pixel radius of the solar disc for the images in Figure 2 and Figure 3, along with an image with high amount of cloud are shown in Table 1. The pixel counting to calculate these percentages does not include the masked pixels hidden by the occultation disc or those outside the image area.

As has been previously found for the Total Sky Imager, the threshold to distinguish between thick and thin cloud will vary with sky conditions and with the camera[18]. Consequently, this threshold can be readily varied within the software as appropriate. The part of the sky not classified due to the masking of the solar disc is of the order of 3.5%. The masking of the solar disc is also employed with the Total Sky Imager and Whole Sky Camera systems to prevent saturation of the charge-coupled device camera and pixel blooming effects in bright sky conditions.

The validation of the smartphone sky camera was undertaken with *Matlab* image processing compared to image classification using a supervised image classification approach with *MultiSpec* for the cases of total cloud, thick cloud and thin cloud for solar zenith angles from 6 to 49 degrees and total cloud from 4% to 98%. For the total cloud, the differences are within 10%. For the thick cloud and thin cloud, the differences are within 15%. These are also the differences for the proximity to the sun clouds in the first two images in Table 1. This second set of differences for the thin cloud are marginally higher due to the subjectivity of distinguishing between thin and thick cloud in the supervised classification and in setting the threshold between thin and thick cloud in the image analysis. This threshold and the threshold for distinguishing between sky and cloud may need small adjustments for different cameras on other smartphones and for different atmospheric conditions. However, this can be readily done using the image analysis algorithm.

The percentages of total cloud, thick cloud and thin cloud in proximity to the solar disc, within a 250 pixel radius are provided in Figure 4 for the images taken in this research. The advantage of providing the percentage of cloud in proximity to the solar disc is that the clouds in proximity to the solar disc have a significant influence on the solar radiation

reaching the surface of the earth, including the potential for enhancement above cloud free conditions[2].

The errors associated with the system developed are comparable to those associated with existing commercial systems and those associated with manual observations. The system described in this paper has the advantage of low cost and the potential for widespread use in research associated with the influence of cloud on renewable energy production. There is also the potential for more widespread use in citizen science investigations[31,36].

Conclusion

A smartphone sky camera and associated image analysis algorithm has been developed and validated for the determination of the percentage of cloud cover. This provides the total cloud cover and the percentage of thick and thin cloud in the image. The system has been validated and tested for a range of cloud types and cloud fractions. Additionally, this system provides the percentage of total cloud and thick and thin cloud in proximity to the solar disc. The size of the error in the percentages of total, thick and thin cloud determined with this system are of a comparable size to the errors in the cloud fraction determined with commercial sky camera systems, where the estimated error of the Total Sky Imager system for total cloud cover is ±10% at least 95% of the time[20]. They are also comparable to the errors associated with manual determination of cloud fraction by trained observers.

The system developed using readily available smartphone imaging technologies has the significant advantage of reduced costs compared to commercial sky cameras and potentially increased temporal frequency of measurements, including use for educational purposes, compared to manual observations by trained human observers. Furthermore, the use of a

greater number of ground based imaging systems has the potential to provide for increased validation of cloud cover measurements made by satellites. The use of a mobile phone image sensor and the computing processing power that is inherent in modern day phones has allowed the generation of a methodology that is low cost, accessible and an accurate means of producing cloud images and cloud fractions. The immediate benefits of such readily available algorithms include the potential to develop improved local ultraviolet index and weather forecasts. Longer term models developed from digitally collected cloud information further contribute toward better understanding local trends in cloud patterns, an important factor that requires consideration for the generation of solar energy. The increased spatial resolution of ground based systems such as those developed from smartphone technologies significantly increases the ubiquity of surface information available for the scientific analysis of these phenomena.

Acknowledgements: The equipment employed in this research was funded by internal University of Southern Queensland grants.

References

1. Calbó, J.; Pages, D.; Gonzalez, J. Empirical Studies of Cloud Effects on UV radiation: A Review. Rev. Geophys. 2005, 43, RG2002 doi:10.1029/2004RG000155.
2. Sabburg, J.; Parisi, A.V. Spectral Dependency of Cloud Enhanced UV Irradiance. Atmos. Res. 2006, 81, 206-214.
3. Parisi, A.V.; Downs, N. Variation of the Enhanced Biologically Damaging Solar UV due to Clouds. Photchem. Photobiol. Sci. 2004, 3, 643–647.
4. Seckmeyer, G.; Erb, R.; Albold, A. Transmittance of a Cloud is Wavelength-dependent in the UV-range. Geophys. Res. Lett. 1996, 23, 2753-2755.
5. Sabburg, J.M.; Parisi, A.V.; Kimlin, M.G. Enhanced Spectral UV Irradiance: A One Year Preliminary Study. Atmos. Res. 2003, 66 (4), 261-272.
6. Parisi, A.V.; Sabburg, J.; Turner, J.; Dunn, P. Cloud Observations for the Statistical Evaluation of the UV index at Toowoomba, Australia. Int. J. Biomet. 2008, 52, 159-166.
7. World Meteorological Organization (WMO). Guide to Meteorological Instruments and Methods of Observation; World Meteorological Organisation, 1983; WMO No. 8, 5th Edition, Chapter 11: 11.2.
8. Tapakis, R.; Charalambides, A.G. Equipment and Methodologies for Cloud Detection and Classification: A Review. Solar Energy. 2013, 95, 392-400.
9. Shields, J.E.; Johnson, R.; Koehler, T.L. Automated Whole Sky Imaging Systems for Cloud Field Assessment. Proceedings of the Fourth Symposium on Global Change Studies, Boston, 17-22 Jan, 1993; American Meteorological Society.
10. Shields, J.E.; Karr, M.E.; Johnson, R.W.; Burden, A.R. Day/night Whole Sky Imagers for 24-h Cloud and Sky Assessment: History and Overview. J. Appl. Optics. 2013, 52, 1605-1616 doi:10.1364/AO.52.001605.

11. Long, C.N.; Slater, D.W.; Tooman, T. Total Sky Imager (TSI) Model 880 Status and Testing Results. Atmospheric Radiation Measurement Program Tech Report ARM TR-006. 2001. http://www.arm.gov/publications/tech_reports/arm-tr-006.pdf. Accessed Dec 2014.
12. Pfister, G.; McKenzie, R.L.; Liley, J.B.; Thomas, A.; Forgan, B.W.; Long, C.N. Cloud Coverage Based on All-sky Imaging and its Impact on Surface Solar Irradiance. J. Appl. Meteorol. 2003, 42, 1421-1434.
13. Huo, J.; Lu, D.R. Calibration and Validation of an All-sky Imager. Atmos. Oceanic Sci. Lett. 2009, 2, 220-223.
14. Roman, R.; Anton, M.; Cazorla, A.; de Miguel, A.; Olmo, F.J.; Bilbao, J.; Alados-Arboledas, L. Calibration of an All-sky Camera for Obtaining Sky Radiance at Three Wavelengths. Atmos. Meas. Tech. 2012, 5, 2013-2024.
15. Urquhart, B.; Kurtz, B.; Dahlin, E.; Ghonima, M.; Shields, J.E.; Kleissl, J. Development of a Sky Imaging System for Short-term Solar Power Forecasting. Atmos. Meas. Tech. Discuss. 2014, 7, 4859-4907.
16. Sabburg, J.; Wong, J. Evaluation of a Ground-based Sky Camera System for use in Surface Irradiance Measurement. J. Atmos. Oceanic Tech. 1999, 16, 752-759.
17. Sabburg, J.; Wong, J. Evaluation of a Sky/cloud Formula for Estimating UV-B Irradiance under Cloudy Skies. J. Geophys. Res. 2000, 105 (D24), 29,685-29,692.
18. Long, C.N.; Sabburg, J.; Calbó, J.; Pages, D. Retrieving Cloud Characteristics from Ground-based Daytime Color All-sky Images. J. Atmos. Oceanic Tech. 2006, 23, 633-652.
19. Souza-Echer, M.P.; Pereira, E.B.; Bins, L.S.; Andrade, M.A.R. A Simple Method for the Assessment of the Cloud Cover State in High-latitude Regions by a Ground-based Digital Camera. J. Atmos. Oceanic Tech. 2006, 23, 437-447.

20. Sabburg, J.; Long, C.N. Improved Sky Imaging for Studies of Enhanced UV Irradiance. Atmos. Chem. Phys. 2004, 4, 2543-2552.
21. Kassianov, E.; Long, C.N.; Christy, J. Cloud-base-height Estimation from Paired Ground-based Hemispherical Observations. J. Appl. Meteorol. 2005, 44, 1221-1233.
22. Nguyen, D.; Kleissl, J. Stereographic Methods for Cloud Base Height Determination using Two Sky Imagers. Solar Energy, 2014, 107, 495-509.
23. Foyo-Moreno, I.; Alados, I.; Olmo, F.J.; Alados-Arboledas, L. The Influence of Cloudiness on UV Global Irradiance (295-385 nm). Agric. For. Meteorol. 2003, 120, 101-111.
24. National Aeronautics and Space Administration (NASA) MODIS Atmosphere. http://modis-atmos.gsfc.nasa.gov/MOD06_L2/ 2014 Accessed June 2014.
25. Silva, A.A.; Echer, M. Ground Based Measurements of Local Cloud Cover. Meteorol. Atmos. Phys. 2013, 120, 201-212.
26. Cazorla, A.; Olmo, F.J.; Alados-Arboledas, L. Development of a Sky Imager for Cloud Cover Assessment. J. Opt. Soc. Am. A. 2008, 25, 29-39.
27. Heinle, A.; Macke, A.; Srivastav, A. Automatic Cloud Classification of Whole Sky Images. Atmos. Meas. Tech. Discuss. 2010, 3, 269-299.
28. Igoe, D.; Parisi, A.V. Evaluation of a Smartphone Sensor to Broadband and Narrowband Ultraviolet A Radiation. Instrument. Sci. Tech. 2015, DOI:10.1080/10739149.2014.1002039.
29. Igoe, D.; Parisi, A.V.; Carter, B. A Method for Determining the Dark Response for Scientific Imaging with **S**martphones. Instrument. Sci. Tech. 2014, 42, 586-592.
30. Igoe, D.; Parisi, A.V.; Carter, B. Smartphone-based Android App for Determining UVA Aerosol Optical Depth and Direct UVA Irradiances. Photochem. Photobiol. 2014, 90, 233-237.

31. Igoe, D.; Parisi, A.V.; Carter, B. Evaluating UVA Aerosol Optical Depth using a Smartphone Camera. Photochem. Photobiol. 2013, 89, 1244-1248.
32. Igoe, D.; Parisi, A.V.; Carter, B. Characterisation of the UVA Response of a Smartphone. Photochem. Photobiol. 2013, 9, 215-218.
33. Kogan, http://www.kogan.com/au/buy/triple-lens-kit-mobile-phones/ 2015 Accessed April 2015.
34. MathWorks, Inc. Image Types. http://au.mathworks.com/help/matlab/creating_plots/image-types.html. 2014 Accessed 5 Dec 2014
35. MultiSpec. A Freeware Multispectral Image Data Analysis System. https://engineering.purdue.edu/~biehl/MultiSpec/description.html. 2014 Accessed 2 Jan 2014
36. Snik, F.; Rietjens, J.H.H.; Apituley, A.; Volten, H.; Mijling, B.; Di Noia, A.; Heikamp, S.; Heinsbroek, R.C.; Hasekamp, O.P.; Smit, J.M.; Vonk, J.; Stam, D.M.; van Harten, G.; de Boer, J.; Keller, C.U.; 3187 iSPEX Citizen Scientists. Mapping Atmospheric Aerosols with a Citizen Science Network of Smartphone Spectropolarimeters. Geophys. Res. Lett. 2014, 41 doi:10.1002/2014GL061462.

Table 1. The percentages of total cloud, thick and thin cloud in the whole image and within a 250 pixel radius of the sun for the images in Figure 2 and Figure 3 and an image with a high percentage of cloud cover.

Solar Zenith Angle	Whole Image Cloud			Proximity to Sun Cloud		
	Total (%)	Thick (%)	Thin (%)	Total (%)	Thick (%)	Thin (%)
11^o	24.8	12.1	12.7	7.1	2.4	4.7
6^o	58.1	43.6	14.5	72.4	57.1	15.3
38^o	99.4	98.5	0.9	98.8	98	0.8

Figure Captions

Figure 1 – The setup showing the fish eye lens attached to the smartphone and the shadow disc to obscure the sun from the sensor.

Figure 2 - The unprocessed (left) and the processed image (right) with a low amount of cloud taken on 7 Jan 2015 1117 (solar zenith angle of 11^o). The processed images show the thick cloud as white, the thin cloud as green and the sky as blue. The parts of the image that are masked due to the occultation disc or that are outside of the fish eye image area are shown in black, with the centre of the sun depicted by the red dot.

Figure 3 – The unprocessed (left) and the processed image (right) with a mid amount of cloud taken at 7 Jan 2015 1146 (solar zenith angle of 6^o).

Figure 4 - The percentages of total cloud (top graph), thick cloud and thin cloud (bottom graph) in proximity to the solar disc determined from a sample of 40 smartphone images recorded for a solar zenith angle between 6^o and 49^o.

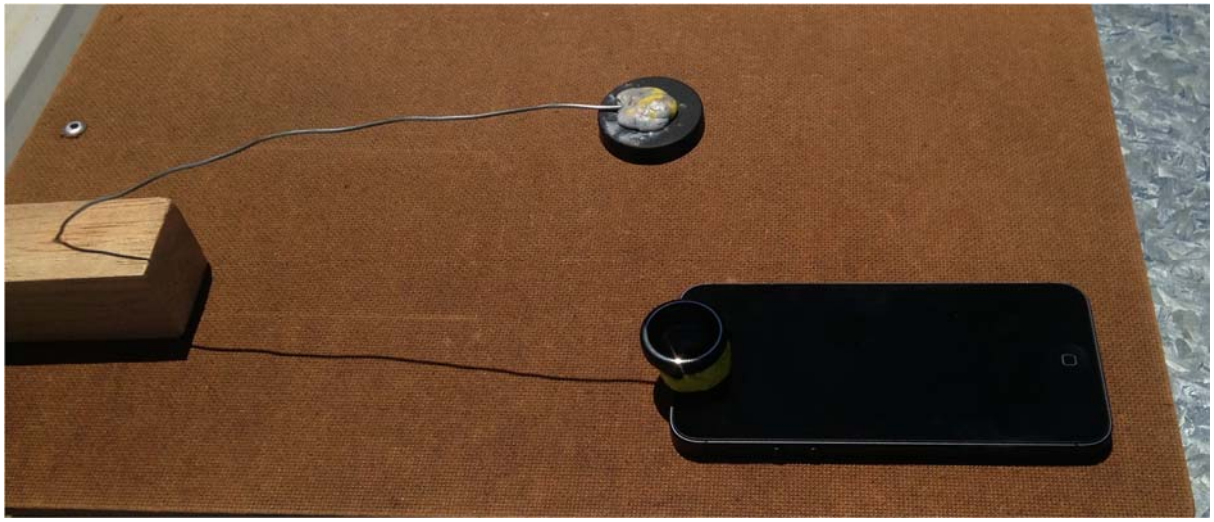

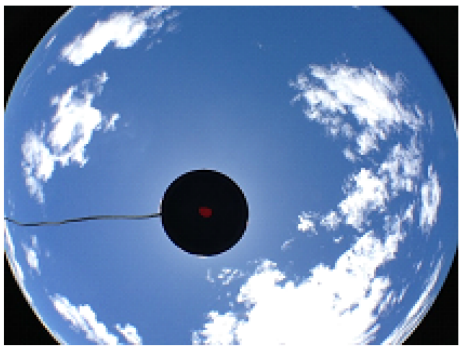

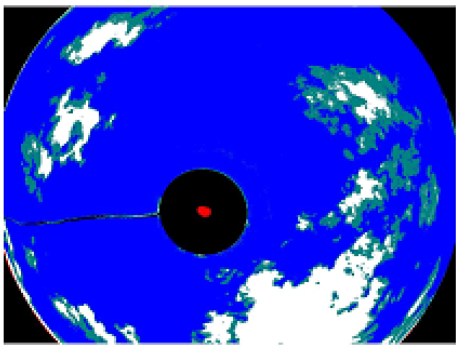

1

2

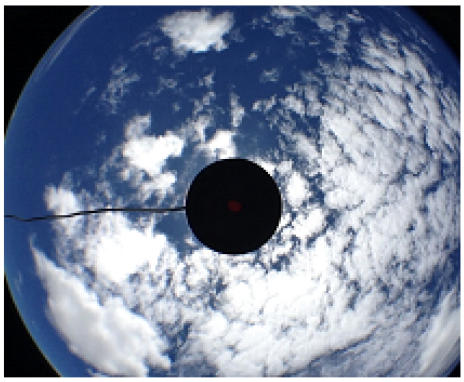

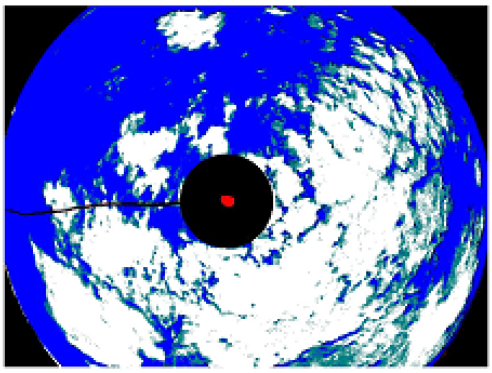

1

2

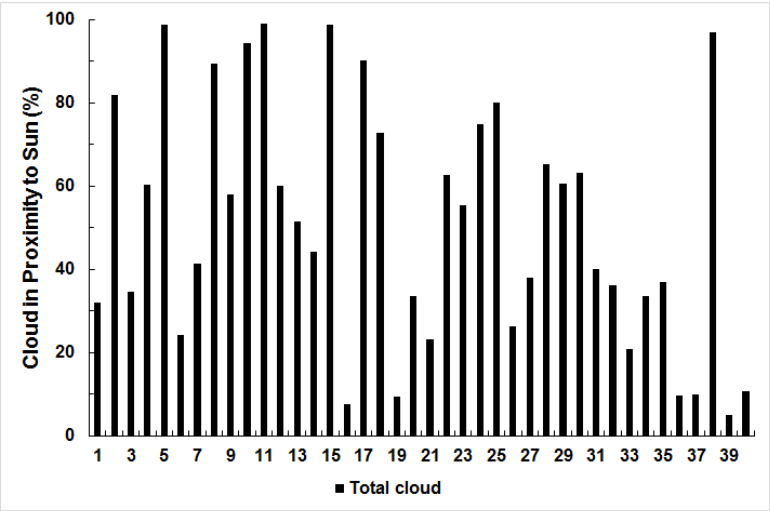
Cloud in Proximity to Sun (%)
100
80
60
40
20
0
1 3 5 7 9 11 13 15 17 19 21 23 25 27 29 31 33 35 37 39
Total cloud

1

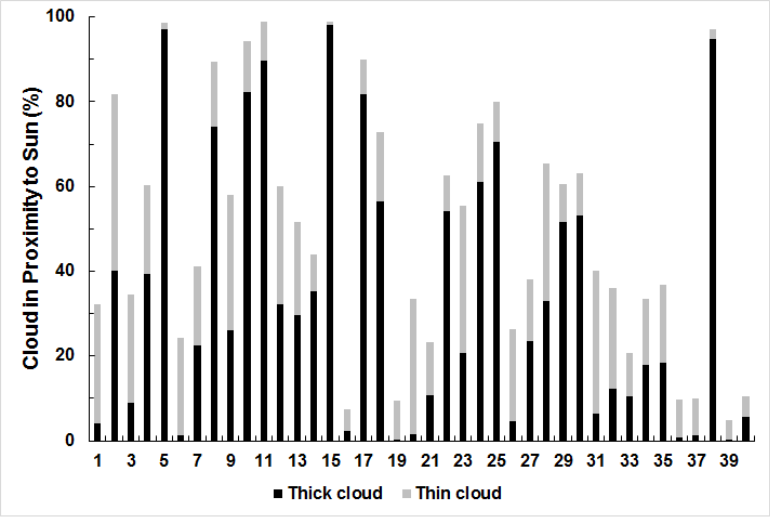
Cloud in Proximity to Sun (%)
100
80
60
40
20
0
1 3 5 7 9 11 13 15 17 19 21 23 25 27 29 31 33 35 37 39
Thick cloud
Thin cloud

2